Available online at www.sciencedirect.com
SCIENCE DIRECT®
Polymer 44 (2003) 5239–5250
polymer
www.elsevier.com/locate/polymer

Effect of hydrolysis on spatial inhomogeneity in poly(acrylamide) gels of various crosslink densities

Mine Yener Kizilay, Oguz Okay*

Department of Chemistry, Istanbul Technical University, 80626 Maslak, Istanbul, Turkey

Received 14 January 2003; received in revised form 27 May 2003; accepted 5 June 2003

Abstract

The spatial inhomogeneity in poly(acrylamide) (PAAm) gels of various crosslink densities has been investigated with the static light scattering measurements. The gels were prepared using *N*,*N*′-methylenebis(acrylamide) (BAAm) as a crosslinker at a fixed initial monomer concentration but at various crosslink densities. Ammonium persulfate-*N*,*N*,*N*′,*N*′-tetramethylethylenediamine (TEMED) redox initiator system was used to initiate the polymerization reactions as well as to create charged groups in the aged gels. The gels were characterized by elasticity tests and by light scattering measurements at a gel state just after their preparation. Elasticity measurements show that 91–94% of the crosslinker molecules used in the hydrogel preparation were wasted in ineffective crosslinks. Debye–Bueche analysis of the light scattering data indicates frozen concentration fluctuations within the gel samples, which increase continuously with increasing crosslink density of the hydrogels. This phenomenon was explained with the multiple crosslinking reactions leading to the formation of highly crosslinked regions in the final hydrogel. The extent of concentration fluctuations was found to decrease drastically with increasing time of aging of gels in the synthesis reactor, indicating that the hydrolysis of amide groups into carboxylate anions facilitates the homogenization of the gel samples. A thermodynamic model was developed to explain the experimental observations in terms of the osmotic pressure of counterions in the aged gels.

Keywords: Poly(acrylamide) gels; Inhomogeneity; Static light scattering

1. Introduction

Hydrogels are important materials of both fundamental and technological interest. They are usually prepared by free-radical crosslinking copolymerization of a monovinyl monomer with a divinyl monomer (crosslinker) in a homogeneous solution. Swelling properties and the elastic behavior of hydrogels have been intensively studied in the last four decades. However, theories are still unable to predict their physical properties from the synthesis conditions. This is due to the several non-idealities of the gel formation system such as the different and conversion-dependent reactivities of the vinyl groups, cyclization, multiple crosslinking, and diffusion-controlled reactions [1,2]. Hydrogels formed in such a non-ideal picture necessarily include defects affecting their physical properties such as swelling, elasticity, transparency, and permeability.

One of the network defects, which have been extensively studied, is the gel inhomogeneity [3,4]. In contrast to the ideal gels with a homogeneous distribution of crosslinks throughout the gel sample, real gels always exhibit an inhomogeneous crosslink density distribution, known as the spatial gel inhomogeneity. Since the gel inhomogeneity is closely connected to the spatial concentration fluctuations, scattering methods such as light scattering [5,6], small-angle X-ray scattering [5,7], and small-angle neutron scattering [8–10] have been employed to investigate the spatial inhomogeneities. The gel inhomogeneity can be manifested by comparing the scattering intensities from the gel and from a semi-dilute solution of the same polymer at the same concentration. The scattering intensity from gels is always larger than that from the polymer solution. The excess scattering over the scattering from polymer solution is related to the degree of the inhomogeneities in gels.

The spatial inhomogeneity in acrylamide (AAm)-based hydrogels has been investigated as a function of a number of parameters, such as the crosslink density [11–14], the type

* Corresponding author. Tel.: +90-212-285-3156; fax: +90-212-285-6386.
E-mail address: okayo@itu.edu.tr (O. Okay).

0032-3861/03/$ - see front matter © 2003 Elsevier Ltd. All rights reserved.
doi:10.1016/S0032-3861(03)00494-4

of the crosslinker [15], the ionization degree [3,4,16], the swelling ratio [4,17], and the temperature [18]. In general, the gel inhomogeneity increases significantly with the crosslink density. A reduced reactivity of the crosslinker used in the hydrogel preparation also leads to a higher degree of inhomogeneity. On the other hand, the inhomogeneity decreases with the ionization degree of gels. An enhancement of the excess scattering is generally observed, if the gel swells beyond its swelling degree after preparation.

It is well known that a poly(acrylamide) (PAAm) gel made by redox polymerization changes to a partially charged gel due to hydrolysis of its amide groups [19]. Ilavsky et al. showed that the gels or solutions of PAAm prepared using *N*,*N*,*N*′,*N*′-tetramethylethylenediamine (TEMED) as the reducing component of the initiator system have a pH value between 8 and 9 [20]. At this pH value, the amide groups on the PAAm chains gradually convert into carboxylate anions with increasing time of aging in the polymerization reactor [20]. The degree of hydrolysis in PAAm solutions has been quantitatively studied by Zurimendi et al. [21]. Mallo et al. investigated the extent of hydrolysis in PAAm gels as a function of aging time [22]. It was shown that the hydrolysis proceeds rather time linearly and results in increase in the swelling degree and in the cooperative diffusion coefficient of aged gels. Takata et al. compared inhomogeneities of a one-month aged PAAm gel with that after a gelation time of 20 h [23]. It was shown that the static inhomogeneities and dynamic fluctuations are smaller in the aged gel compared to the gel after preparation.

Here, we report a systematic study of the effect of aging time of PAAm gels on the extent of spatial gel inhomogeneity. For this purpose, we prepared a series of PAAm gels of various crosslink densities. The gels were characterized at various aging times by static light scattering measurements at a gel state just after their preparation. An equivalent semi-dilute PAAm solution served as a reference in the understanding of the inhomogeneities in gels. The excess scattering from the gels is taken as a measure of their inhomogeneity. A thermodynamic model was developed to explain the observed phenomena in terms of the osmotic pressure of mobile counterions in the hydrolyzed PAAm gels.

2. Experimental

2.1. Synthesis of hydrogels

AAm (Merck), BAAm (Merck), ammonium persulfate (APS, Merck), potassium persulfate (KPS, Merck) and TEMED were used as received. PAAm gels were prepared by free-radical crosslinking copolymerization of AAm and BAAm in an aqueous solution at 24 °C in the presence of 2.63 mM APS initiator and 0.375 v/v% TEMED accelerator. The initial monomer concentration was fixed at 5 w/v% while the amount of the crosslinker BAAm was varied between at 0 and 3 mol%. The reaction time was one day. Details about the gel synthesis have been reported elsewhere [24,25]. PAAm solutions were prepared in the same way as the gels, but BAAm was not added to the initial mixture. For comparison, gels and solutions of PAAm were prepared under the same initial monomer concentration except that TEMED was not used. The polymerization and crosslinking reactions were initiated at 40 °C using 0.474 mM KPS initiator.

The degree of dilution of the networks after their preparation was denoted by v_2^0, the volume fraction of crosslinked polymer after the gel preparation. In order to determine v_2^0, PAAm hydrogels after preparation were first swollen in water to extract non-polymerizable or soluble components and then dried at 90 °C under vacuum for at least two weeks. Assuming that the monomer conversions were complete after the crosslinking copolymerization, the theoretical value of v_2^0 can also be calculated from the initial molar concentration of the monomers [24,25]. Measurements showed that the experimental value of v_2^0 is close to its theoretical value of 0.037, indicating that, under the reaction conditions, the monomer conversions and the gel fractions were complete.

2.2. Mechanical measurements

Uniaxial compression measurements were performed on gels just after their preparation. All the mechanical measurements were conducted in a thermostated room of 24 ± 0.5 °C. The stress–strain isotherms were measured by using an apparatus previously described [26]. Briefly, a cylindrical gel sample of about 6 mm in diameter and 7 mm in length was placed on a digital balance (Sartorius BP221S, readability and reproducibility: 0.1 mg). A load was transmitted vertically to the gel through a road fitted with a PTFE end-plate. The compressional force acting on the gel was calculated from the reading of the balance. The resulting deformation was measured after 20 s of relaxation by using a digital comparator (IDC type Digimatic Indicator 543-262, Mitutoyo Co.), which was sensitive to displacements of 10^{-3} mm. The measurements were conducted up to about 15% compression. Reversibility of the isotherms was tested by recording the force and the resulting deformation during both force-increasing and force-decreasing processes. The two processes yielded almost identical stress–strain relations. From the repeated measurements, the standard deviations in the modulus value were less than 3%. The sample weight loss during the measurements due to water evaporation was found to be negligible. The elastic modulus G_0 was determined from the slope of linear dependence $f = G_0(\alpha - \alpha^{-2})$, where f is the force acting per unit cross-sectional area of the undeformed gel specimen, and α is the deformation ratio (deformed length/initial length). Typical stress–strain dependencies of

the hydrogels prepared at 5 w/v% initial monomer concentration but at various crosslinker contents are shown in Fig. 1.

2.3. Light scattering experiments

For the light scattering measurements, the crosslinking polymerizations were carried out in the light scattering vials. All glassware was kept dustfree by rinsing in hot acetone prior using. The solutions were filtered through membrane filters (pore size = 0.2 μm) directly into the vials. This process was carried out in a dustfree glovebox. All the gels subjected to light scattering measurements were clear and appeared homogeneous to the eye. For the calculation of excess scattering from gels, all the crosslinking polymerizations were repeated under the same experimental conditions except that the crosslinker BAAm was not used. The aging of both PAAm gels and solutions was carried out at 24 ± 0.5 °C in vials, in which they were formed.

The light scattering measurements were carried out at 24 ± 0.5 °C using a commercial multi-angle light scattering DAWN EOS (Wyatt Technologies Corporation) equipped with a vertically polarized 30 mW Gallium–arsenide laser operating at $\lambda = 690$ nm and 18 simultaneously detected scattering angles. The scattered light intensities from gels and solutions of PAAm of various aging times were recorded from 42.8 to 142.5°, which correspond to the scattering vector q range $8.8 \times 10^{-4} - 2.3 \times 10^{-3}$ Å^{-1}, where $q = (4\pi n/\lambda)\sin(\theta/2)$, θ the scattering angle, λ the wavelength of the incident light in vacuum, n the refractive index of the medium, which is 1.34. The light scattering system was calibrated against a toluene standard. During the measurements with gel samples, the vial was rotated eight times between each cycle of data sampling.

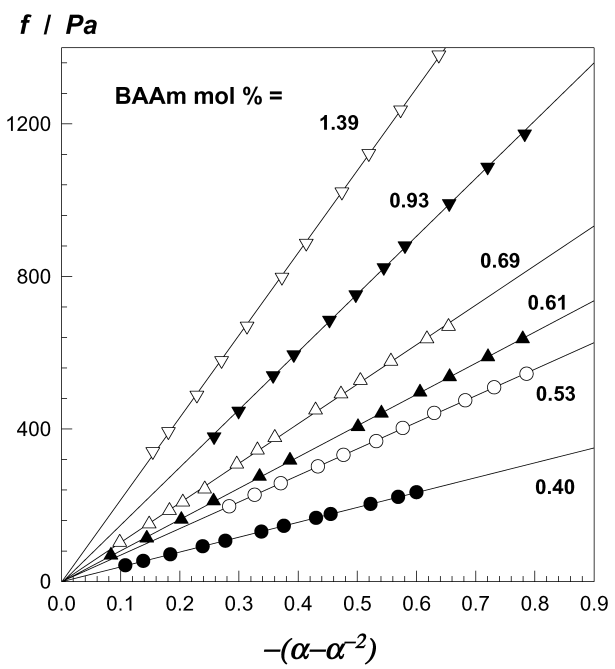

Fig. 1. Typical stress–strain data for PAAm hydrogels just after their preparation. The mole percent of BAAm in the feed is indicated in the Figure. Temperature = 24 °C.

3. Results and discussion

We discuss the results of our experiments in three subsections. In Section 3.1, spatial inhomogeneity in PAAm gels of various crosslink densities is discussed. In Section 3.2, the variation of the extent of the gel inhomogeneity depending on the time of aging of gels is discussed. In Section 3.3, a thermodynamic model is presented to interpret the experimental observations.

3.1. Effect of crosslink density

In Fig. 2, the elastic modulus of gels after preparation G_0 is shown as a function of the crosslinker (BAAm) content. As expected, G_0 is an increasing function of the crosslinker concentration. Assuming that all BAAm molecules used in the hydrogel synthesis participate in forming effective crosslinks, theoretical elastic modulus G_{theo} of the hydrogels can be calculated as [27,28]:

$$G_{\text{theo}} = A\frac{2\rho X}{M_r}RTv_2^0 \tag{1}$$

where the front factor A equals to 1 for an affine network and $1 - 2/\phi$ for a phantom network, ϕ is the functionality of the crosslinks, ρ is the polymer density (1.35 g/ml) and M_r is the

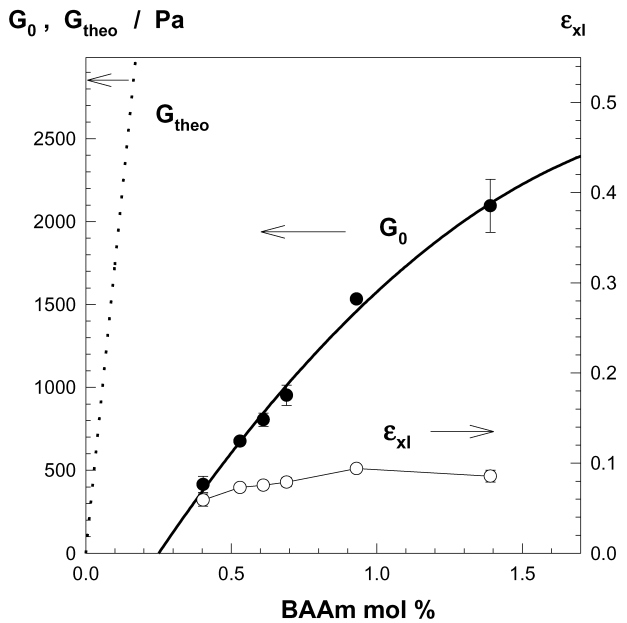

Fig. 2. The elastic modulus of gels after preparation G_0 (filled symbols) and the crosslinking efficiency of BAAm ϵ_{xl} (open symbols) shown as a function of the crosslinker (BAAm) content. The theoretical elastic modulus G_{theo} vs BAAm mol% plot is shown by the dotted curve. Temperature = 24 °C.

molecular weight of repeat unit (71 g/mol), X is the crosslinker ratio (mole ratio of BAAm to AAm), R and T are in their usual meanings. Previous works show that the phantom network theory of elasticity adequately describes the stress–strain behavior of PAAm gels [29]. Assuming phantom network behavior ($\phi = 4$), G_{theo} of the hydrogels calculated using Eq. (1) are also shown in Fig. 2 as the dotted curve. It is seen that G_{theo} is much higher than G_0 of the hydrogels. The crosslinking efficiency of BAAm $\epsilon_{xl} = G_0/G_{theo}$, that is the fraction of BAAm forming effective crosslinks is shown in the Figure as open symbols. ϵ_{xl} is in the range 0.06–0.09, indicating that 91–94% of BAAm used in the hydrogel preparation were wasted. This value is in good agreement with that found from the equilibrium swelling measurements of gels [30,31] as well as from the determination of the pendant vinyl group content of pregel polymers [32,33]. This high fraction of wasted BAAm originates from the characteristics of AAm-BAAm copolymerization [1]. As reported in the literature, the reactivity ratios of AAm and BAAm monomers are 0.57 and 3.4, respectively [34]. Thus, in copolymerization, the growing chains in the pregel regime are rich in BAAm units. Furthermore, these chains are highly diluted by the solvent and the monomer at low conversion so that cyclization predominates in the early stages of the reaction. Present results indeed show that a significant fraction of BAAm is consumed by cyclization reactions during the gel formation process.

Light scattering measurements were carried out on hydrogels prepared in the range of BAAm between 0 and 2 mol%. The hydrogels prepared above 2 mol% BAAm became first translucent and then opaque during the gel formation reactions. It is obvious that these gels have heterogeneities in a spatial scale of submicrometer to micrometer. Therefore, only gel samples with less than 2% BAAm were subjected to light scattering measurements.

The measurements were conducted after one day of polymerization time. Excess scattering intensities from gels $R_{ex}(q)$ were calculated as $R_{ex}(q) = R_{gel}(q) - R_{sol}(q)$, where $R_{gel}(q)$ and $R_{sol}(q)$ are the Rayleigh ratios for gel and polymer solution, respectively. Fig. 3A and B show $R_{gel}(q)$ and $R_{ex}(q)$ vs the scattering vector q plots for PAAm hydrogels of various BAAm contents, respectively. It is seen that the gels scatter much more light than the corresponding polymer solution of the same concentration. This is in accord with the results reported earlier [5,14]. Interestingly, even the presence of a small amount of the crosslinker BAAm results in increased scattered light intensities from the gel samples. The excess scattering from gels increases with increasing BAAm content. Since $R_{ex}(q)$ is a measure of the spatial inhomogeneity in a gel, this indicates that the PAAm gel becomes more inhomogeneous with increasing BAAm concentration. Furthermore, at low BAAm content, the excess scattering is nearly q-independent but for higher BAAm content, the q dependence becomes more

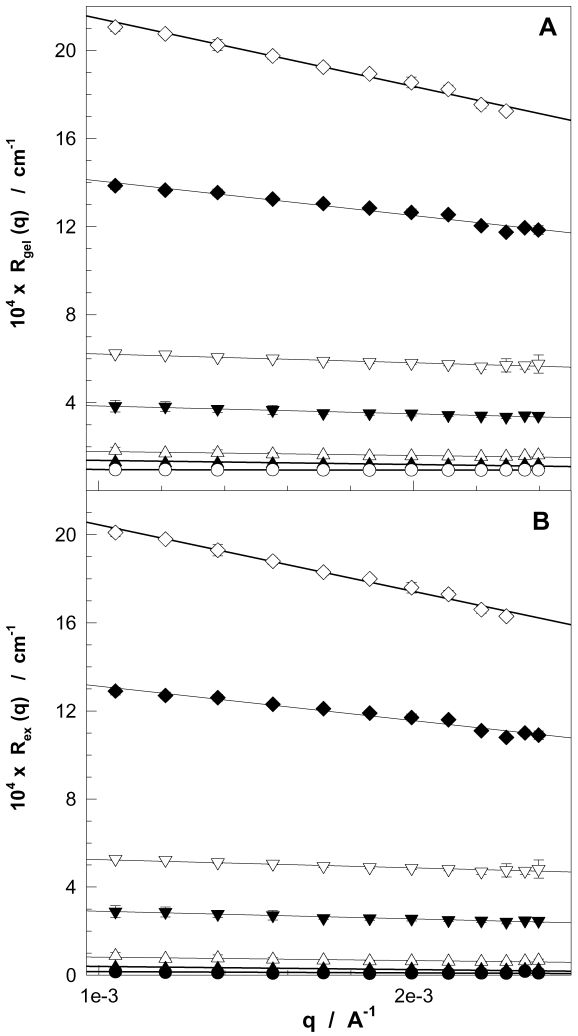

Fig. 3. Scattering light intensities from gels $R_{gel}(q)$ (A) and the excess scattering $R_{ex}(q)$ (B) vs scattering vector q plots for PAAm gels of various crosslinker contents. BAAm mol % = 0(○), 0.10 (●), 0.23 (▲), 0.54 (△), 1.14 (▼), 1.46 (▽), 1.86 (◆), and 1.94 (◇).

pronounced. To compare the excess scattering of different gels, we will focus on the scattering intensity measured at a fixed scattering vector $q = 1 \times 10^{-3}$ Å^{-1}. Fig. 4 shows the excess scattering at $q = 1 \times 10^{-3}$ Å^{-1} ($R_{ex,q}$) plotted as a function of BAAm%. $R_{ex,q}$ increases first slightly up to about 1.5 mol% BAAm but then rapidly increases with a further increase in BAAm concentration. As shown in the inset to Fig. 4, a good linear behavior was obtained if the data points are redrawn in a semi-logarithmic plot, indicating an exponential law between $R_{ex,q}$ and BAAm%. This suggests the occurrence of a phase separation in the gel samples as the crosslinker content is increased.

To interpret light scattering results from gels, several functional forms of excess scattering $R_{ex}(q)$ have been proposed empirically, i.e. Debye–Bueche [35–38], Guinier [39–42], and Ornstein–Zernicke functions [39–43]. For

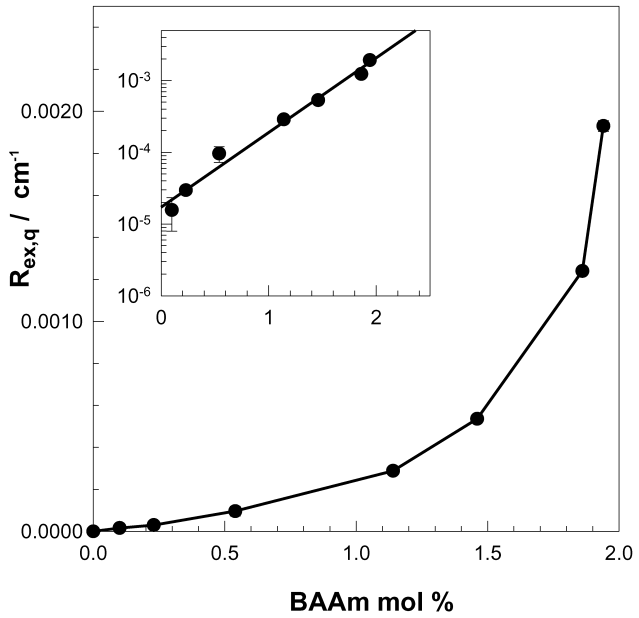

Fig. 4. The excess scattering $R_{ex,q}$ measured at $q = 1 \times 10^{-3}$ Å^{-1} shown as a function of BAAm mol%. The inset shows the same data in a semi-logarithmic plot.

example, the excess scattering was given by the Debye–Bueche function as:

$$R_{ex}(q) = \frac{4\pi K \xi^3 \langle \eta^2 \rangle}{(1 + q^2 \xi^2)^2} \tag{2}$$

where K being the optical constant, $K = 8\pi^2 n^2 \lambda^{-4}$, ξ is the correlation length of the scatterers, and $\langle \eta^2 \rangle$ is the mean square fluctuation of the refractive index. Note that the correlation length ξ of the Debye–Bueche theory is a characteristic length scale in the gel. It shows the average distance over which the local variation in the polymer concentration can be considered not to change appreciably. Thus, ξ is a measure of the spatial extent of the fluctuation [37,38]. The larger the ξ values, the larger are the extension of the inhomogeneities. Since scatterers in gels are highly crosslinked regions, the correlation length corresponds to the size of these regions.

According to Eq. (2), the slope and the intercept of $R_{ex}(q)^{-1/2}$ vs q^2 plot (Debye–Bueche plot) give ξ and $\langle \eta^2 \rangle$ of a gel sample, i.e.

$$(R_{ex}(q))^{-\frac{1}{2}} = \underbrace{\left(2\sqrt{\pi K \xi^3 \langle \eta^2 \rangle}\right)^{-1}}_{\text{intercept = b}} + \underbrace{\frac{1}{2}\sqrt{\frac{\xi}{\pi K \langle \eta^2 \rangle}}}_{\text{slope = a}} q^2 \tag{2a}$$

$$\xi = \left(\frac{a}{b}\right)^{0.5} \tag{2b}$$

and

$$\langle \eta^2 \rangle = (4\pi K a^{1.5} b^{0.5})^{-1} \tag{2c}$$

In Fig. 5, some of the data points are replotted in the form of Debye–Bueche plots. It is seen that straight lines are obtained in this analysis, indicating that the Debye–Bueche function works well. In fact, ln $R_{ex}(q)$ vs q^2 and $R_{ex}(q)^{-1}$ vs q^2 plots also give straight lines, implying that the Guinier and Ornstein–Zernicke functions also work well. The values of ξ and $\langle \eta^2 \rangle$ were calculated from the Debye–Bueche analysis. The standard deviations in ξ and $\langle \eta^2 \rangle$ values were always less than 5%. The correlation length of the scatterers ξ was found to be 16 ± 3 nm and slightly decreasing function of BAAm concentration. The mean square fluctuations $\langle \eta^2 \rangle$ are in the range 10^{-7}–10^{-5} and they increase with BAAm content. Thus, increasing concentration fluctuations $\langle \eta^2 \rangle$ decrease the correlation length ξ of PAAm gels. This inverse relation between ξ and $\langle \eta^2 \rangle$ was also reported before for PAAm gels [5,15]. This is due to the fact that, increasing crosslink density of the highly crosslinked regions of a gel leads to the deswelling of these regions so that their size ξ decreases on rising $\langle \eta^2 \rangle$.

The semi-logarithmic plot in Fig. 6 showing BAAm% dependence of the mean square fluctuations $\langle \eta^2 \rangle$ indicates a power law behavior. Thus, Debye–Bueche method shows that the correlation length, i.e. the extension of the inhomogeneities in PAAm gels slightly decreases while the extent of the fluctuations $\langle \eta^2 \rangle$ rapidly increases with increasing BAAm content. Similar results were also obtained by fitting the data to the Guinier and Ornstein–Zernicke functions.

As pointed out in the Introduction, cyclization and multiple crosslinking reactions are the main features of the gel formation process of PAAm gels. These reactions are

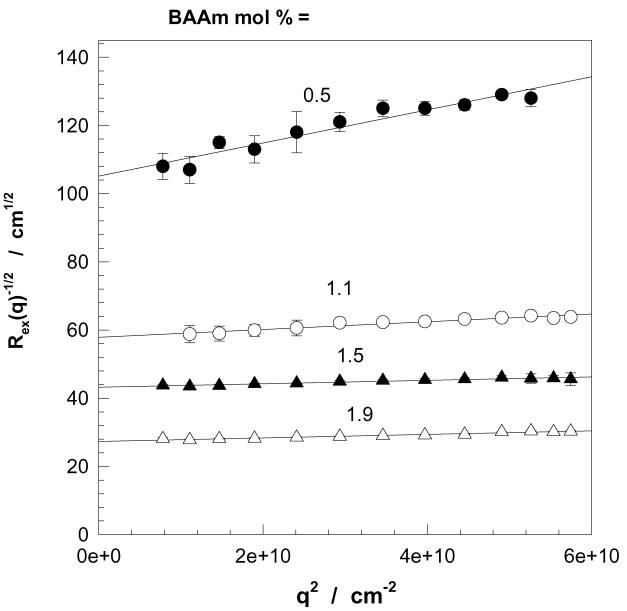

Fig. 5. Debye–Bueche plots for PAAm gels prepared at various BAAm mol% indicated in the Figure.

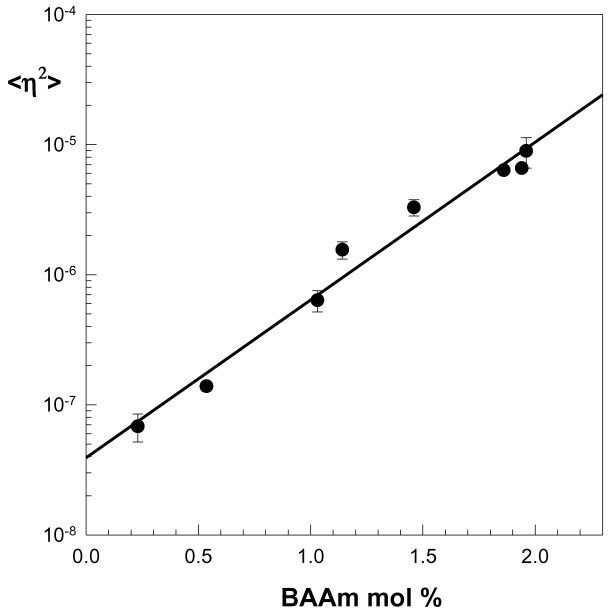

Fig. 6. The mean square fluctuation of the refractive index $\langle \eta^2 \rangle$ in PAAm gels shown as a function of BAAm mol%. The error bars indicate standard deviations obtained from measurements on at least five different gel samples; if not seen, they are smaller than the symbols themselves.

schematically illustrated in Fig. 7. With cyclization, the cycle is formed when the macroradical attacks the pendant vinyl groups in the same kinetic chain; while with multiple crosslinking, it is formed if the radical attacks double bonds pendant on other chains already chemically connected with the growing radical [44–47]. Important point is that cycles are intramolecular links and therefore, they do not contribute to the rubber elasticity of polymer networks and thus, to the concentration fluctuations of gels. However, multiple crosslinks are elastically effective links in a small region of space. The regions, where the multiple crosslinks form, have a higher crosslink density then do others so that they will not swell as much as the other regions (Fig. 7). As a result, the inhomogeneous distribution of effective crosslinks and the resulting concentration fluctuations $\langle \eta^2 \rangle$ in the hydrogels are a result of multiple crosslinking reactions. At low crosslinker contents, since the local pendant vinyl group concentration surrounding the growing macroradical is relatively low, only a few multiple crosslinks is expected to occur after each crosslinking reaction. However, at high crosslinker contents, the possibility of multiple crosslinkages is enhanced due to the high pendant vinyl group concentration (Fig. 7). Indeed, previous results show that, at relatively high BAAm contents, about 2×10^3 multiple crosslinks occur after each single crosslink [33]. This leads to the formation of highly crosslinked regions in the final hydrogel. Thus, the higher the crosslinker content, the larger the number of multiple crosslinks will be and the greater the extent of gel inhomogeneity.

3.2. Effect of hydrolysis

Hydrolysis of PAAm gels prepared with TEMED is known to proceed almost linearly with the time of aging [22]. Thus, as the time goes on, more and more AAm units are converted into the acrylic acid (AAc) units so that the gel becomes increasingly ionic. Ilavsky et al. showed that the fraction of AAc units increases from 0 to 0.052 with increasing aging time up to 103 days while the molar mass of linear PAAm's prepared under the same experimental condition remains constant [20]. Their elasticity measurements also show that the elastic moduli of gels do not change much with increasing aging time of gels [20]. Thus, aging of PAAm gels only influences the hydrolysis degree of the network chains.

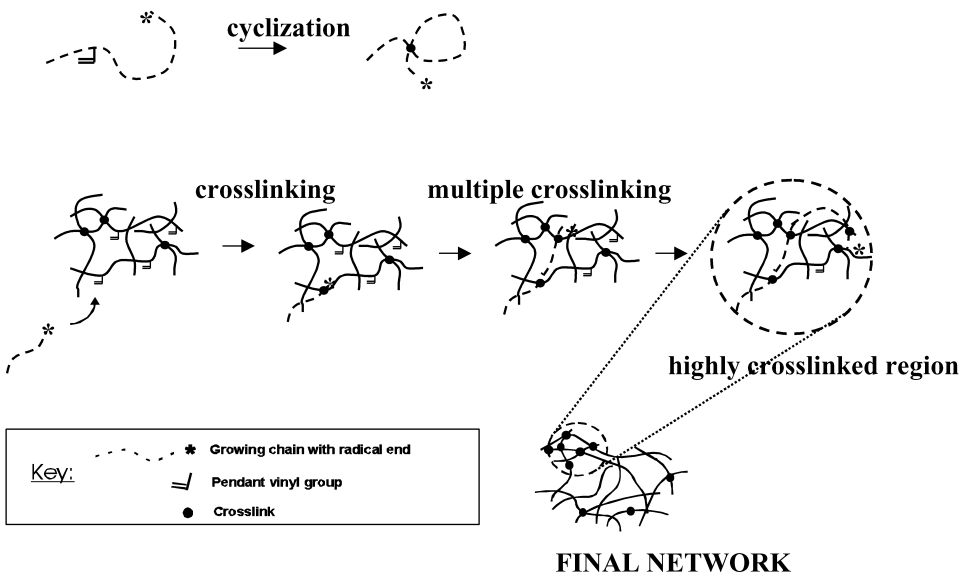

Fig. 7. Schematic representation of cyclization and multiple crosslinking reactions in free-radical crosslinking copolymerization. The area inside the dotted circle is a highly crosslinked region in the final network, which forms due to the multiple crosslinkages.

In the present work, gels and solutions of PAAm were left in vials at 24 °C, in which they were formed for various times up to 160 days. The excess scattering intensities from gels with respect to polymer solutions having the same aging time were measured. Fig. 8A–D show $R_{ex}(q)$ vs q plots for PAAm hydrogels at various aging times. BAAm contents of gels are indicated in the Figure. The excess scattering decreases, i.e. PAAm gel becomes increasingly homogeneous with increasing time of aging at all crosslinker contents studied. Furthermore, the excess scattering, which was q-dependent at high crosslinker contents, becomes nearly q-independent at long aging times. In Fig. 9A, the excess scattering $R_{ex,q}$ at $q = 1 \times 10^{-3}$ Å^{-1} is plotted as a function of aging time for various BAAm%. $R_{ex,q}$ decreases first rapidly up to about 30 days then slightly with increasing aging time. The double-logarithmic $R_{ex,q}$ vs aging time plots given in Fig. 9B show that the decrease in $R_{ex,q}$ with time i.e. the homogenization of PAAm gels becomes faster as the crosslinker content is increased.

The scattered light intensities from aged gels were interpreted using the Debye–Bueche analysis. As in Section 3.1, linear $R_{ex}(q)^{-1/2}$ vs q^2 plots were obtained, from which the parameters $\langle\eta^2\rangle$ and ξ were calculated. $\langle\eta^2\rangle$ and ξ of gels are collected in Fig. 10 plotted as a function of the aging time. It is seen that, both $\langle\eta^2\rangle$ and ξ do not change much up to about 5 days. At longer aging times, the correlation length of the scatterers ξ increases while the mean square fluctuations $\langle\eta^2\rangle$ decrease rapidly. The measurements were also repeated using gel samples prepared without using TEMED. The results obtained at various crosslink densities showed no change in both $\langle\eta^2\rangle$ and ξ values with the time of aging up to 110 days. Thus, the presence of TEMED, i.e. the hydrolysis is responsible for the homogenization of gels during aging.

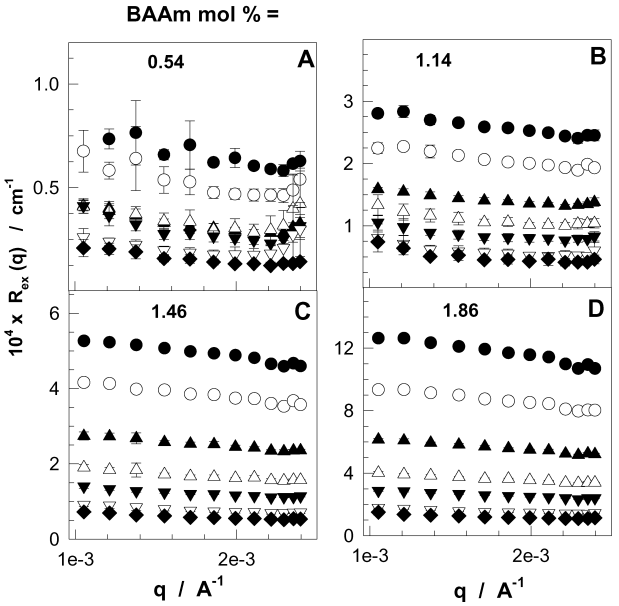

Fig. 8. The excess scattering $R_{ex}(q)$ vs scattering vector q plots for PAAm gels at various BAAm mol% indicated in the Figure. The aging times are 1 (●), 6 (○), 14 (▲), 32 (△), 54 (▼), 109 (▽), and 160 days (◆).

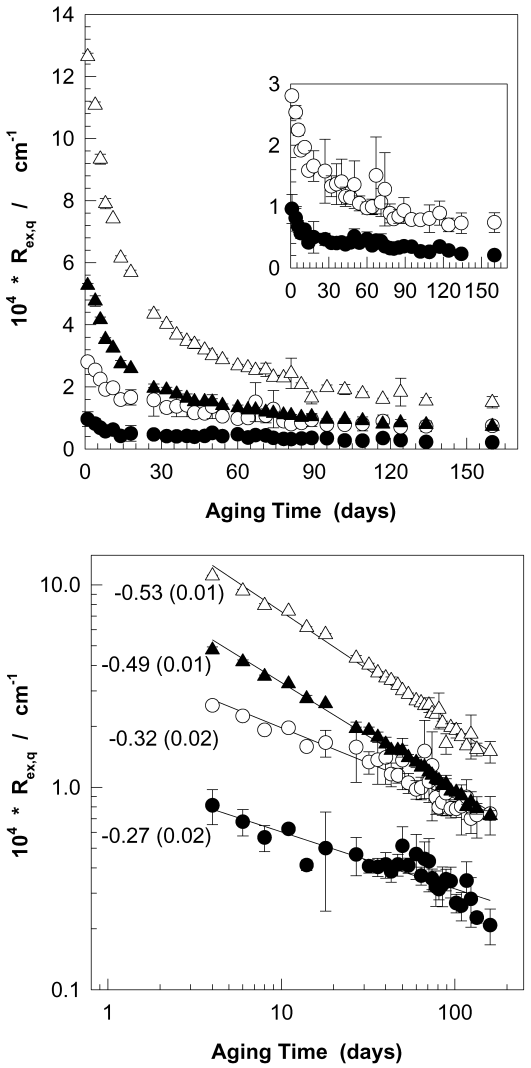

Fig. 9. (A) The excess scattering $R_{ex,q}$ measured at $q = 1 \times 10^{-3}$ Å^{-1} shown as a function of the time of aging. BAAm mol% = 0.54 (●), 1.14 (○), 1.46 (▲), and 1.86 (△). The data points obtained at 0.54 and 1.14 mol% BAAm are also shown in the inset at a larger scale. (B) The double-logarithmic $R_{ex,q}$ vs aging time plots of the data shown in (A). The slopes and the standard deviations of the least-squares lines through the data are indicated in the Figure.

The experimental results may be attributed to the rearrangement of the network chains in aged gels due to the electrostatic interactions. As the charge density of the network chains increases, they rearrange themselves as far as possible due to the repulsion of the charged groups. Those of the chains in the dense regions, that are relatively mobile, move apart to assume a new structure [48]. According to this picture, the decrease in excess scattering, that is, the homogenization of gels during aging must proceed faster at low crosslinker contents due to the fact that the more mobile chains can easily move to take this new structure. However, the experimental results show opposite behavior (Fig. 9B). The higher the crosslinker content, the

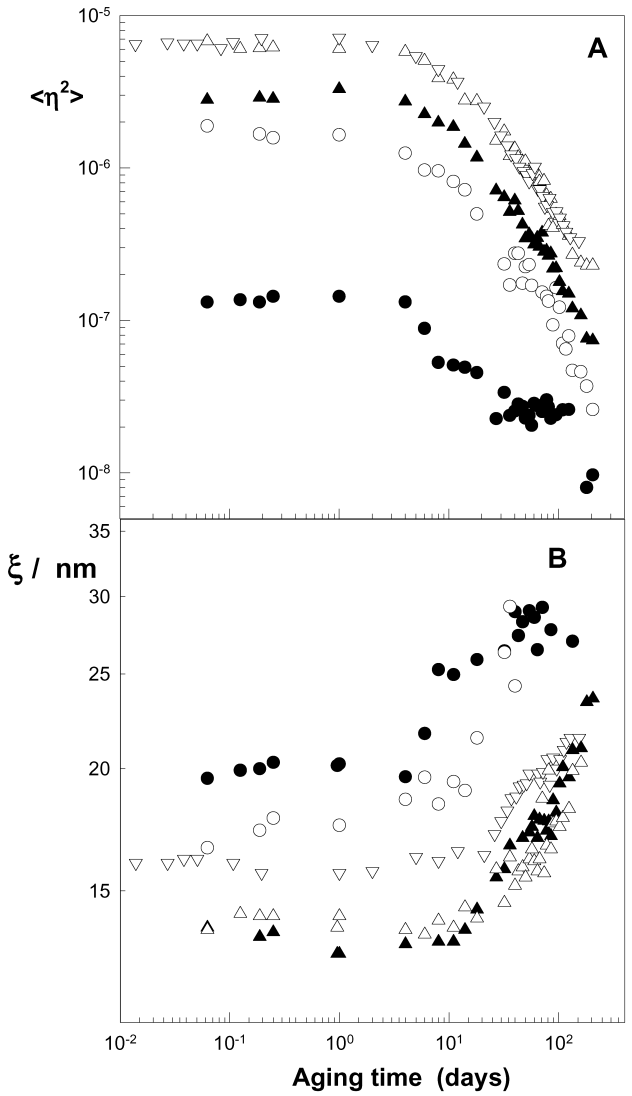

Fig. 10. The mean square fluctuation of the refractive index $\langle \eta^2 \rangle$ and the correlation length of the scatterers ξ in PAAm gels shown as a function of the time of aging. BAAm mol%: 0.54 (●), 1.14 (○), 1.46 (▲), 1.86 (△), and 1.94 (▽).

faster the homogenizing move of the network chains out of the dense regions. Thus, the results cannot be explained with the electrostatic interactions of the charged groups. A more plausible explanation is the swelling of the dense regions of gel due to the inhomogeneous distribution of mobile counterions in aged gels. This is illustrated schematically in Fig. 11. As shown in Section 3.1, PAAm gel consists of highly crosslinked (dense) regions, which are interconnected by the less crosslinked (dilute) interstitial regions. Thus, the gel consists of regions of high and low polymer concentrations. At a given degree of hydrolysis, the local charge density (the number of ionic units per unit gel volume) will thus be higher in the dense regions compared to the dilute regions. Due to the condition of electroneutrality, the concentration of the mobile counterions will also be higher in the dense regions. This unequal distribution of counterions between the inside and outside the dense regions of gel will create an osmotic pressure resulting in the swelling of the dense regions. This means that, upon ionization, water diffuses from dilute to the dense regions of the gel due to the additional osmotic pressure of excess counterions. As a result, the size of the dense regions ξ increases while the extent of the concentration fluctuations $\langle \eta^2 \rangle$ decreases with increasing degree of hydrolysis.

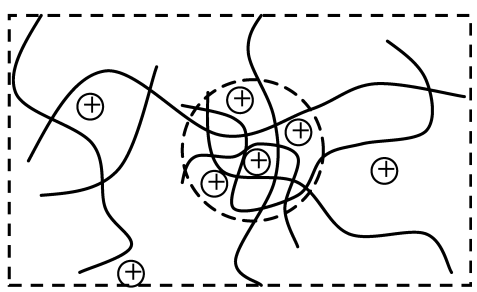

Fig. 11. Schematic representation of the dense and dilute regions of an aged PAAm gel. Mobile counterions (cations) are shown by (+).

3.3. Thermodynamic modeling of homogenization of gels during hydrolysis

In this section, we present a thermodynamic model to calculate, on a microscopic scale, the concentration fluctuations in gels depending on the degree of hydrolysis. We categorize the various regions of an inhomogeneous gel as being either dense or dilute. Dense regions are highly crosslinked and they are distributed randomly throughout the gel volume. We assume that each dense region of gel is homogeneous and the network chains are long enough to apply the Gaussian statistics. Since the crosslink density of the dense regions is larger than the average, these regions of gel partially shrink to ensure a micro-swelling equilibrium with the solvent in the environment. The dilute region is less crosslinked and the swelling capacity of this region is higher than the degree of dilution after the gel preparation. Thus, this region of gel is not in thermodynamic equilibrium. If a good solvent is added, only the dilute region will swell further to attain the swelling equilibrium.

Let us choose randomly a microscopic portion of a gel sample, as illustrated in Fig. 11. Let v_2^g and v_2^s be the volume fractions of crosslinked polymer in the dense and dilute regions, respectively, and v_e^g be the crosslink density of the dense region. Note that, in our notation, the symbols with the superscripts g and s denote the properties of dense and dilute regions, respectively. The equilibrium state properties of the dense region will be analyzed using the Flory–Rehner (FR) theory of swelling equilibrium. According to the FR theory, the osmotic pressure π of a gel is the sum of three contributions [49,50]:

$$\pi = \pi_{mix} + \pi_{el} + \pi_{ion} \tag{3}$$

where π_{mix}, π_{el}, and π_{ion} are the osmotic pressures due to

polymer–solvent mixing, due to deformation of network chains to a more elongated state, and due to the non-uniform distribution of mobile counterions between the dense and the dilute regions of the gel, respectively. According to the Flory–Huggins (FH) theory, π_{mix} is given by [27]:

$$\pi_{mix} = -\frac{RT}{V_1}[\ln(1 - v_2^g) + v_2^g + \chi(v_2^g)^2] \quad (4)$$

where χ is the polymer–solvent interaction parameter and V_1 is the molar volume of solvent. The FR and FH theories contain several assumptions that have been the subject of much discussion. The validity of these assumptions is beyond the scope of the present paper. To describe the elastic contribution π_{el}, we will use the phantom network model for tetrafunctional networks [27]. Since the dense region of gel is in thermodynamic equilibrium with the solvent, the volume fraction of polymer in the reference state equals to the equilibrium volume fraction of polymer. π_{el} is then given by:

$$\pi_{el} = -\frac{1}{2}RTv_e^g v_2^g \quad (5)$$

During hydrolysis, fixed charges start to appear on the network chains, which are confined to the dense and dilute regions, along with an equal number of counterions. Ionic contribution π_{ion} to the swelling pressure is caused due to the concentration difference of the counterions between the dense and dilute regions of the gel, represented by C^g and C^s, respectively:

$$\pi_{ion} = RT(C^g - C^s) \quad (6)$$

The condition of electroneutrality requires the equality $C = C_{fix}$ in both dense and dilute regions of gel, where C_{fix} is the concentration of fixed charges, i.e.

$$C_{fix} = \frac{i}{V_1}v_2 \quad (7)$$

where i is the effective charge density, i.e. the mole fraction of the charged units in the network chains. Thus, Eqs. (6) and (7) lead to:

$$\pi_{ion} = \frac{iRT}{V_1}(v_2^g - v_2^s) \quad (8)$$

According to Eq. (8), the osmotic pressure of counterions increases with increasing degree of hydrolysis or, with increasing concentration difference between the dense and dilute regions. Substitution of Eqs. (4), (5) and (8) into Eq. (3) and since the osmotic pressure π equals to zero at swelling equilibrium, one obtains the following equation for the dense region of an inhomogeneous gel:

$$\ln(1 - v_2^g) + v_2^g + \chi(v_2^g)^2 + 0.5V_1 v_e^g v_2^g - i(v_2^g - v_2^s) = 0 \quad (9)$$

By substituting $i = 0$ into Eq. (9), one obtains the swelling equation for the dense region of gel before the onset of hydrolysis:

$$\ln(1 - v_{2,0}^g) + v_{2,0}^g + \chi(v_{2,0}^g)^2 + 0.5V_1 v_e^g v_{2,0}^g = 0 \quad (9a)$$

where the symbols with the subscript 0 denote the initial properties.

Due to the concentration difference of mobile counterions between the inside and outside the dense region, water diffuses from dilute to the dense region as the degree of hydrolysis increases. As a result, the polymer volume fraction v_2^g in the dense region will decrease starting from its initial values of $v_{2,0}^g$, while v_2^s will increase starting from $v_{2,0}^s$. Although the network chains in both regions change their configurations during swelling or shrinking, they are fixed in their locations, i.e. they cannot escape out of their regions. This means that the polymer volumes in both regions remain constant during hydrolysis. If x represents the volume fraction of the dense region in gel, from the material balance, we may write:

$$xv_2^g = x_0 v_{2,0}^g \quad (10a)$$

$$(1 - x)v_2^s = (1 - x_0)v_{2,0}^s \quad (10b)$$

where x_0 is the value of x at $i = 0$. Combining Eqs. (10a) and (10b) to eliminate x, one obtains:

$$v_2^s = \frac{v_{2,0}^s(1 - x_0)}{1 - x_0 v_{2,0}^g / v_2^g} \quad (11)$$

Simultaneous solutions of Eqs. (9) and (11) give the concentration fluctuation $(v_2^g - v_2^s)$ in a microscopic portion of a gel sample depending on the degree of hydrolysis. Assuming linear additivity of the refractive indices of the solvent n_1 and the polymer n_2, the refractive indices of the dense and dilute regions, N^g and N^s, respectively, can then be calculated as follows:

$$N^g = \Delta n v_2^g + n_1 \quad (12a)$$

$$N^s = \Delta n v_2^s + n_1 \quad (12b)$$

where $\Delta n = n_2 - n_1$. By defining η^2 as the fluctuations in refractive index $(N^g - N^s)^2$ at a given point of gel, one obtains:

$$\eta^2 = \Delta n^2(v_2^g - v_2^s)^2 \quad (13)$$

which becomes before the onset of hydrolysis:

$$\eta_0^2 = \Delta n^2(v_{2,0}^g - v_{2,0}^s)^2 \quad (13a)$$

Note that η^2 represents the refractive index fluctuations for a given spatial configuration in gel, while $\langle\eta^2\rangle$ of the Debye–Bueche theory is the ensemble average measurement, that is, one averaged over a large number of spatial configurations existing in the gel.

3.4. Calculations

The system specific parameters used were $n_1 = 1.33$, $n_2 = 1.5$ [51], $\chi = 0.48$ [29,52], and $V_1 = 1.8 \times 10^{-5}$ m^3 mol^{-1}.

Respective calculations showed that η^2 is rather insensitive to the initial volume fraction of dense regions x_0. x_0 was set to 0.01 for the following calculations. The degree of hydrolysis i, the crosslink density of the dense region ν_e^g, and the initial value of the fluctuations η_0^2 were taken as the independent parameters. The following procedure was used for calculations:

(1) Eq. (9a) was solved for the initial polymer volume fraction in the dense region $\nu_{2,0}^g$,
(2) Eq. (13a) was solved together with the value $\nu_{2,0}^g$ for the initial polymer volume fraction in the dilute region $\nu_{2,0}^s$,
(3) After finding the initial concentrations $\nu_{2,0}^g$ and $\nu_{2,0}^s$, Eqs. (9) and (11) were solved simultaneously for ν_2^g and ν_2^s as a function of i as the independent parameter. Eq. (13) was then solved for the fluctuations in the refractive index η^2.

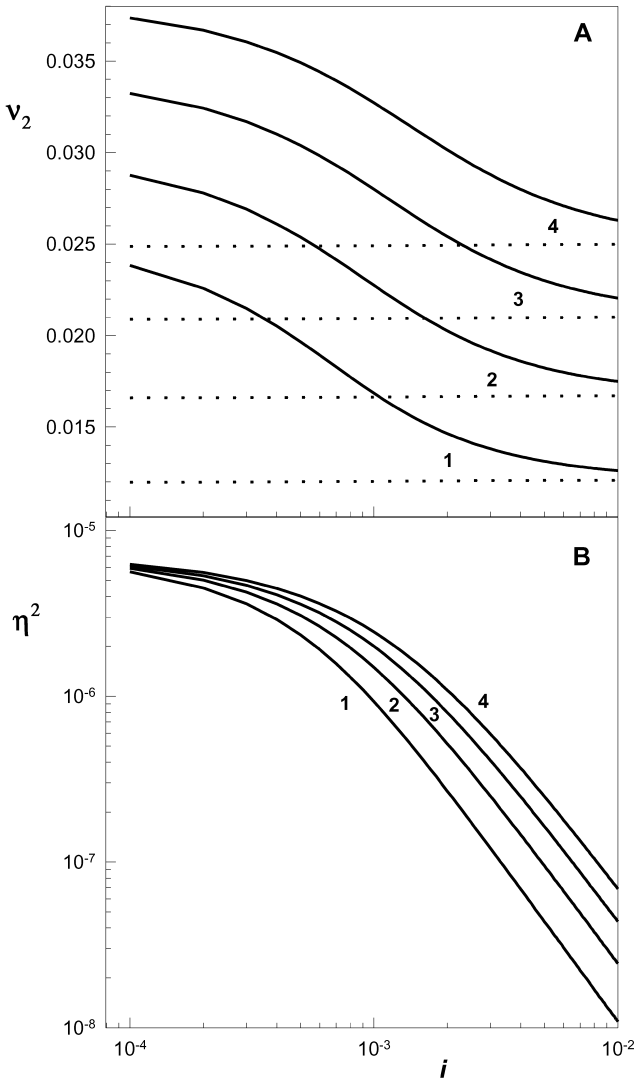

Fig. 12. (A) Variations of the polymer concentrations in the dense (solid curves) and dilute regions of a gel (dotted curves) with the network charge density i. (B) Variation of the square fluctuations in the refractive index η^2 with the network charge density i. Calculations were for $x_0 = 0.01$, $\eta_0^2 = 7 \times 10^{-6}$ and for various crosslink densities ν_e^g of the dense regions. $\nu_e^g = 80$ (1), 100 (2), 120 (3), and 140 mol m^{-3} (4).

In Fig. 12A, ν_2^g (solid curves) and ν_2^s (dotted curves) vs i plots are presented for various values of ν_e^g. Calculations were for $\eta_0^2 = 7 \times 10^{-6}$. For the same gel systems, η^2 vs i plots are given in Fig. 12B. It is seen that the polymer concentration in the dense region of gel ν_2^g decreases while that in the dilute region ν_2^s slightly increases as the charge density of the network i is increased. At high charge densities, ν_2^g approaches to ν_2^s, i.e. the gel becomes

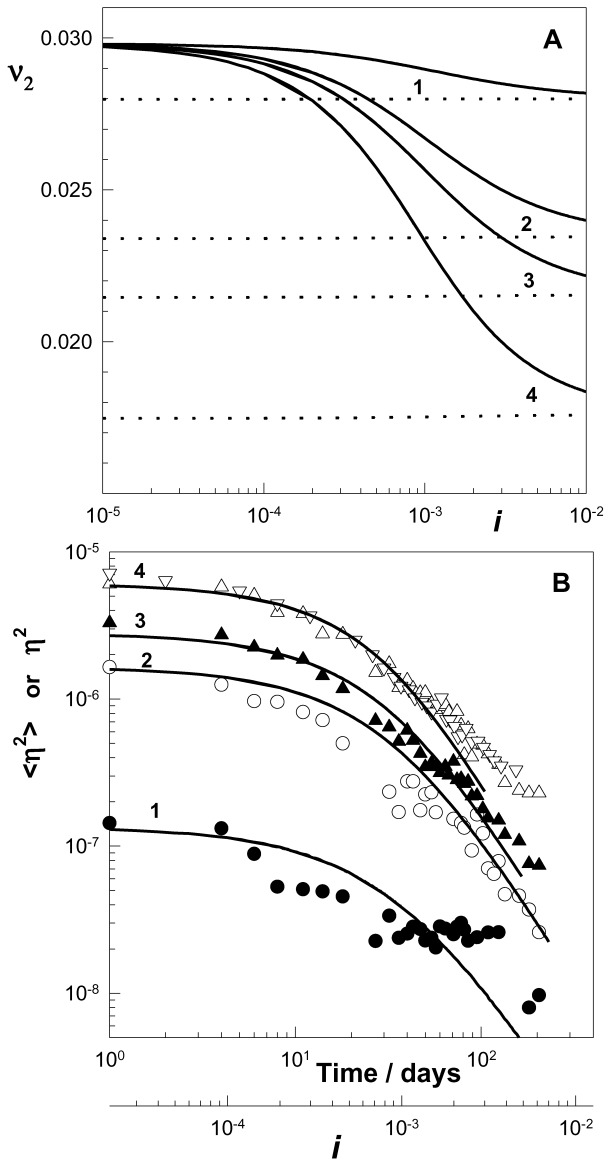

Fig. 13. (A) Variations of the polymer concentrations in the dense (solid curves) and dilute regions of a gel (dotted curves) with the network charge density i. (B) Variation of the square fluctuations in the refractive index η^2 with the network charge density i (solid curves). Calculations were for $x_0 = 0.01$ and $\nu_e^g = 100$ mol m^{-3}. $\eta_0^2 = 1.35 \times 10^{-7}$ (1), 1.65×10^{-6} (2), 2.8×10^{-6} (3), 6.1×10^{-6} (4). For comparison, experimental $\langle\eta^2\rangle$ vs aging time data of PAAm gels are also shown in the Figure as symbols. BAAm mol%: 0.54 (●), 1.14 (○), 1.46 (▲), 1.86 (△), and 1.94 (▽).

homogeneous, as seen in Fig. 12B. At a given degree of hydrolysis i, the extent of gel inhomogeneity η^2 decreases with increasing ν_e^g because of the increased crosslink density of both the dense and the dilute regions. In Fig. 13A, ν_2^g and ν_2^s vs i plots are shown for $\nu_e^g = 100$ mol m^{-3} and for various values of η_0^2. η_0^2 values used in the calculations were taken as the mean-square fluctuations $\langle\eta^2\rangle$ of PAAm gels after their preparation (Fig. 10A). As η_0^2 of gels increases, ν_2^g decreases more rapid, i.e. homogenization becomes faster. This is in accord with the results given in Section 3.3. In Fig. 13B, the fluctuations in the refractive index η^2 are shown as the solid curves plotted as a function of i. For comparison, the experimental $\langle\eta^2\rangle$ vs aging time data are also shown as symbols. In this Figure, the independent parameter i of the model was adjusted to fit the experimental data, which is equivalent to fitting the Y-intercept in Fig. 10A. It is seen that the model predictions well reproduce our experimental observations.

It must be noted that several assumptions and restrictions were introduced during the development of the model. The network chains in the dense regions of gel may show deviations from the Gaussian behavior, especially at high crosslinker contents. Moreover, the local degree of swelling of a dense region will also depend on the properties of neighboring regions because it is encapsulated in a matrix environment. Therefore, the actual swelling degree of a dense region will be less than predicted by the model. However, the idealized model presented is though to form the basis for treating these deviations.

4. Conclusions

The spatial inhomogeneity in PAAm gels has been investigated with the static light scattering measurements. The gels were prepared at a fixed initial monomer concentration but at various crosslink densities. The use of TEMED as the accelerator during the gel formation process enabled us to create charged groups in the aged gels. Elasticity measurements show that 91–94% of the crosslinker molecules used in the hydrogel preparation were wasted in ineffective crosslinks. Debye–Bueche analysis of the light scattering data indicates that the frozen concentration fluctuations within PAAm gel samples increase continuously with increasing crosslink density. This phenomenon was explained with the multiple crosslinking reactions leading to the formation of highly crosslinked regions in the final hydrogel. It was found that the extent of gel inhomogeneity decreases drastically with increasing aging time, indicating that the hydrolysis of amide groups into acrylate groups facilitates the homogenization of the gels. A thermodynamic model was developed, which takes into account the inhomogeneous distribution of the mobile counterions throughout the gel volume. It was shown that the model predictions well reproduce the experimental observations.

Acknowledgements

Work was supported by the State Planning Organization (DPT).

References

[1] Funke W, Okay O, Joos-Muller B. Adv Polym Sci 1998;136:139.
[2] Okay O. Prog Polym Sci 2000;25:711.
[3] Shibayama M. Macromol Chem Phys 1998;199:1.
[4] Bastide J, Candau SJ. In: Cohen Addad JP, editor. Physical properties of polymeric gels. Wiley; 1996. p. 143.
[5] Mallam S, Horkay F, Hecht AM, Geissler E. Macromolecules 1989; 22:3356.
[6] Ikkai F, Shibayama M. Phys Rev E 1997;56:R51.
[7] Cohen Y, Ramon O, Kopelman IJ, Mizraki S. J Polym Sci Polym Phys Ed 1992;30:1055.
[8] Schosseler F, Skouri R, Munch JP, Candau SJ. J Phys II 1994;4:1221.
[9] Shibayama M, Tanaka T, Han CC. J Chem Phys 1992;97:6842.
[10] Horkay F, McKenna GB, Deschamps P, Geissler E. Macromolecules 2000;33:5215.
[11] Shibayama M, Ikkai F, Nomura S. Macromolecules 1994;27:6383.
[12] Shibayama M, Ikkai F, Shiwa Y, Rabin YJ. Chem Phys 1997;107: 5227.
[13] Ikkai F, Iritani O, Shibayama M, Han CC. Macromolecules 1998;31: 8526.
[14] Hecht AM, Duplessix R, Geissler E. Macromolecules 1985;18:2167.
[15] Lindemann B, Schröder UP, Oppermann W. Macromolecules 1997; 30:4073.
[16] Moussaid A, Candau SJ, Joosten JGH. Macromolecules 1994;27: 2102.
[17] Bastide J, Mendes Jr. E. Makromol Chem Macromol Symp 1990;40: 81.
[18] Takata S, Norisuye T, Shibayama M. Macromolecules 2002;35:4779.
[19] Tanaka T. Phys Rev Lett 1978;40:820.
[20] Ilavsky M, Hrouz J, Stejskal J, Bouchal K. Macromolecules 1984;17: 2868.
[21] Zurimendi JA, Guerrero SJ, Leon V. Polymer 1984;25:1314.
[22] Mallo P, Candau S, Cohen C. Polym Commun 1985;26:232.
[23] Takata SI, Norisuye T, Shibayama M. Macromolecules 1999;32:3989.
[24] Durmaz S, Okay O. Polymer 2000;41:3693.
[25] Gundogan N, Melekaslan D, Okay O. Macromolecules 2002;35:5616.
[26] Sayil C, Okay O. Polymer 2001;42:7639.
[27] Flory PJ. Principles of polymer chemistry. Ithaca, NY: Cornell University Press; 1953.
[28] Treloar LRG. The physics of rubber elasticity. Oxford: University Press; 1975.
[29] Baker JP, Hong LH, Blanch HW, Prausnitz JM. Macromolecules 1994;27:1446.
[30] Okay O, Sariisik SB. Eur Polym J 2000;36:393.
[31] Okay O, Balimtas NK, Naghash HJ. Polym Bull 1997;39:233.
[32] Naghash HJ, Okay O. J Appl Polm Sci 1996;60:971.
[33] Tobita H, Hamielec AE. Polymer 1990;31:1546.
[34] Baselga J, Llorente MA, Hernandez-Fuentes I, Pierola IF. Eur Polym J 1989;25:477.
[35] Debye PJ. J Chem Phys 1959;31:680.
[36] Bueche F. J Colloid Interface 1970;33:61.
[37] Debye P, Bueche AM. J Appl Phys 1949;20:518.
[38] Soni VK, Stein RS. Macromolecules 1990;23:5257.
[39] Horkay F, Hecht AM, Geissler E. Macromolecules 1994;27:1795.
[40] Shibayama M, Tanaka T. J Chem Phys 1992;97:6829.
[41] Wu W, Shibayama M, Roy S, Kurokawa H, Coyne LD, Nomura S, Stein RS. Macromolecules 1990;23:2245.

[42] Higgins JS, Benoit HC. Polymers and neutron scattering. Oxford: Clarendon Press; 1994.
[43] Baumgaertner A, Picot CE. Molecular basis of polymer networks. Berlin: Springer Verlag; 1989.
[44] Okay O, Kurz M, Lutz K, Funke W. Macromolecules 1995;28:2728.
[45] Elliott JE, Bowman CN. Macromolecules 1999;32:8621.
[46] Elliott JE, Anseth JW, Bowman CN. Chem Eng Sci 2001;56:3173.
[47] Elliott JE, Bowman CN. Macromolecules 2001;34:4642.
[48] Skouri R, Schosseler F, Munch JP, Candau SJ. Macromolecules 1995; 28:197.
[49] Flory PJ, Rehner Jr. J. J Chem Phys 1943;11:521.
[50] Frenkel J. Rubber Chem Technol 1940;13:264.
[51] Ying Q, Wu G, Chu B, Farinato R, Jackson L. Macromolecules 1996; 29:4646.
[52] Durmaz S, Okay O. Polymer 2002;43:1215.